Inorganic Chemistry

pubs.acs.org/IC

Article

Synthesis, Structure, and Spectroscopic Study of Redox-Active Heterometallic Cluster-Based Complexes $[Re_5MoSe_8(CN)_6]^n$

Viktoria K. Muravieva,* Ivan P. Loginov, Taisiya S. Sukhikh, Maxim R. Ryzhikov, Vadim V. Yanshole, Vladimir A. Nadolinny, Vincent Dorcet, Stéphane Cordier, and Nikolay G. Naumov

Cite This: *Inorg. Chem.* 2021, 60, 8838−8850

Read Online

ACCESS | Metrics & More | Article Recommendations | Supporting Information

ABSTRACT: The heterometallic cluster-based compound $K_5[Re_5MoSe_8(CN)_6]$ was obtained by high-temperature reaction from a mixture of $ReSe_2$ and $MoSe_2$ in molten potassium cyanide. The redox behavior of the $[Re_5MoSe_8(CN)_6]^{5-}$ cluster anion was studied by cyclic voltammetry in aqueous and organic media showing two reversible one-electron-redox transitions with $E_{1/2}$ of −0.462 and 0.357 V versus Ag/AgCl in CH_3CN. Aqueous media potentials were found to be noticeably shifted to higher values because of solvation. Chemically accessible potentials allowed us to structurally isolate and characterize the $[Re_5MoSe_8(CN)_6]^n$ (n = 3−, 4−, and 5−) cluster complex in several charge states with corresponding cluster skeletal electron (CSE) numbers ranging from 24 to 22. The electronic absorption of the $[Re_5MoSe_8(CN)_6]^n$ cluster complex varies significantly upon a change of the CSE number, especially in the visible and near-IR regions. The local cluster core distortion upon electron removal was confirmed by density functional theory calculation, while the overall geometry of the cluster anion remained practically unaltered.

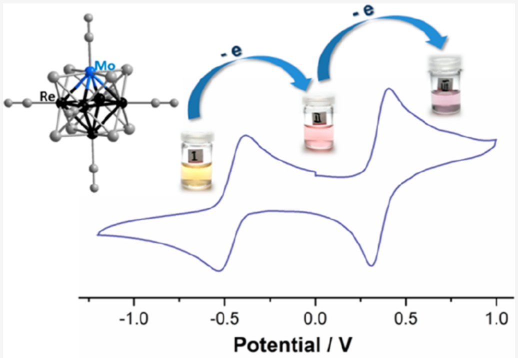

INTRODUCTION

Inorganic high-valence octahedral cluster complexes are known for their promising intrinsic features, among which photoluminescence, radiopacity, biological activity, and catalytic properties have received attention for different application fields.[1−7] The rigidity and stability of the octahedral cluster complexes have been utilized in the design of hybrid materials and extended polymeric solids.[8,9] A typical octahedral cluster consists of a fragment of six covalently bound metal atoms stabilized by inner and apical ligand coordination (Figure 1).

Many octahedral cluster complexes neutral or charged have been found to participate in electron transitions and exhibit redox activity in solution, among which the clusters of tantalum,[10,11] tungsten,[12−14] niobium,[15,16] molybdenum,[17−19] rhenium,[20,21] and technetium[22−24] can be mentioned. In some of the studies, it was shown that variation of the cluster charge by redox reaction leads to significant changes in its absorption spectra.[18,25−30] The joint redox and optical absorption behavior of the octahedral cluster complexes has attracted attention recently in the field of electrochromic light-filtering materials.[31,32] The nature of the metal atoms forming the cluster substantially determines its redox ability and optical properties because of the large contribution of d orbitals of metal to the frontier molecular orbitals of the cluster.[33−38] Only some of the cluster redox transition products for M = Mo, W, Ta, and Nb were isolated as individual compounds because of the large potentials required.[16,18,30,39] Well-known rhenium octahedral

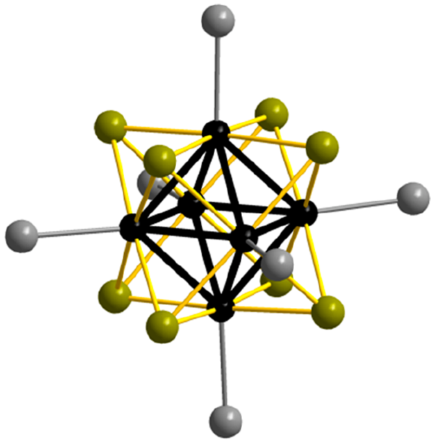

Figure 1. Typical structure of the octahedral cluster complex $[M_6Q^i_8L^a_6]^n$.

Received: March 12, 2021
Published: May 31, 2021

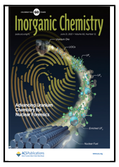

https://doi.org/10.1021/acs.inorgchem.1c00763

cyanocluster-based complexes $[Re_6Q_8(CN)_6]^n$ (Q = S, Se, Te; n = 3− and 4−) mostly exhibit single one-electron oxidation with mild accessible potentials[40,41] accompanied by a drastic change in the optical absorption in the visible region and a respective cluster color change.[29,42,43] The redox transition of the cluster complex proceeds, showing no significant change of the cluster complex interatomic distances,[42] and was performed reversibly in a solid polymer without its degradation ($[\{Gd(H_2O)_3\}_2(fdc)Re_6Se_8(CN)_6]/[\{Gd(H_2O)_3\}_2(fdc)Re_6Se_8(CN)_6]Br$, where fdc = furan-2,5-dicarboxylate).[44] Several examples show that nonisovalent substitution of the cluster metals with the formation of heterometallic clusters can strongly affect the number of redox transitions and their potential values. Heterometallic rhenium cluster-based complex $[Re_4Os_2Se_8(CN)_6]^{2-}$[45] and that recently studied by our group, $[Re_3Mo_3Se_8(CN)_6]^{4-}$,[46] exhibit multiple redox transitions in a relatively narrow potential window also were accompanied by a cluster color change. The presence of several accessible color states can be beneficial in the field of polychromic materials for electrochromic display technologies.[47]

Taking into account the promising features of heterometallic rhenium clusters, further evaluation of the mutual redox and optical absorption of rhenium/molybdenum chalcogenide cluster complexes is of great interest for the present research. Herein, we present synthetic routes, redox, and spectroscopic study of the cluster complex $[Re_5MoSe_8(CN)_6]^n$ (n = 3−, 4−, and 5−) as a novel member of the redox-active cluster series $[Re_{6-x}Mo_xSe_8(CN)_6]^n$ (x = 0−3, 6; n = 3−, ..., 8−).

■ EXPERIMENTAL SECTION

Materials and Methods. Metal diselenides were prepared using the procedure described below. Other reagents and solvents were used as purchased. ***Caution!*** *KCN should be handled with care and decomposes rapidly upon contact with acids and slowly upon contact with water, moisture, or carbon dioxide, producing highly toxic hydrogen cyanide.*

$MoSe_2$ (3.779 g, 0.039 mol) of molybdenum with 6.221 g (0.079 mol) of selenium and $ReSe_2$ (7.334 g, 0.039 mol) of rhenium with 6.221 g (0.079 mol) of selenium were loaded into separate quartz ampules. The ampules were evacuated, sealed, heated at a rate of 1.5 °C/min up to 500 °C, and kept at this temperature for 10 h, then the temperature was raised to 800 °C at a rate of 1 °C/min, and the ampules were heated at this temperature for 48 h. The ampules were cooled to room temperature at a rate of 2.5 °C/min and opened. The phase purity of the products was verified using powder X-ray diffraction (PXRD; Figures S1 and S2). The heavy-element ratios by energy-dispersive spectroscopy (EDS) were 1.0:2.0 Mo/Se and 1.0:2.1 Re/Se.

Elemental analysis was performed with Thermo Fisher Flash 1112 CHNS/O and Euro EA 3000 CHNS analyzers. EDS was performed on a JEOL JSM-7100F field-emission scanning electron microscope and a TM-300 with Bruker Nano EDS analyzer. Fourier transform infrared (FT-IR) spectra in KBr pellets were recorded on Bruker Scimitar FTS 2000 and SIMEX FT-801 spectrometers in the range 4000−375 cm^{-1}. UV−vis absorption measurements were performed in the wavelength range 190−1050 nm on an Agilent Cary 60 UV−vis spectrophotometer. Diffuse-reflectance spectroscopy (DRS) spectra were registered by means of a Shimadzu 3101 PC UV−vis−near-IR (NIR) spectrometer, and the spectra were transformed by the Kubelka−Munk theory equation.[48] High-resolution electrospray ionization mass spectrometry (HR-ESI-MS) was carried out on a high-resolution Bruker maXis 4G ESI-q-TOF mass spectrometer (negative-ion mode, range m/z 300−3000, direct injection with an automatic syringe 0.18 mL/h, voltage +2800 V, nebulizer pressure 1 bar, dry gas 4 L/min, and dry gas temperature 180 °C) at the Center of Collective Use "Mass spectrometric investigations" SB RAS. Electron paramagnetic resonance (EPR) measurements were carried out on a Varian E-109 EPR spectrometer in the X frequency range at 77 K. The EPR spectrum of 2,2′-diphenyl-1-picrylhydrazyl (DPPH) with g = 2.0036 was used as a reference for the g factor. Cyclic voltammetry (CV) was carried out on an Elins P-20X8 voltammetry analyzer using a three-electrode scheme with glassy carbon working, Pt auxiliary, and Ag/AgCl/3.5 M KCl reference electrodes. Investigations were carried out for a 2.5×10^{-3} M solution of cluster salt **2** in a 0.1 M solution of Bu_4NClO_4 in CH_3CN and cluster salt **1** with concentration 9.0×10^{-3} M in a 0.1 M solution of NaCl in H_2O under an Ar atmosphere. The registered value of $E_{1/2}$ for the $Fc^{+/0}$ couple was 0.440 V under the same conditions. PXRD patterns of the synthesized compounds were recorded using a Philips PW1820/1710 diffractometer (Cu Kα 1.54060 Å radiation, graphite monochromator; a Si plate was used as an external standard). Simulated patterns were generated by *PowderCell 2.4* software.[49]

Single-Crystal X-ray Diffraction (XRD) Studies. Single-crystal XRD data for compounds **1**−**4** were collected at 150 K with a Bruker D8 Venture diffractometer [λ(Mo Kα) = 0.71073 Å, mirror optics]. Integration and absorption corrections were applied with the use of the *APEX3* program and processed with the *APEX* 3 program suite.[50] Frame integration and data reduction were carried out with the program *SAINT*.[51] The program *SADABS*[52] was employed for multiscan absorption corrections. The crystal structures were solved using *SHELXT*[53] and refined using *SHELXL*[54] with *OLEX2 GUI*[55] for structures **1**, **3**, and **4**. Structure **2** was solved by a dual-space algorithm using the *SHELXT*[53] program and then refined with full-matrix least-squares methods based on F^2 (*SHELXL*).[54] All non-H atoms were refined with anisotropic atomic displacement parameters. The statistical distribution of Re and Mo was processed in accordance with the EDS data. The occupancy of the Re and Mo atoms for **1**, **3**, and **4** was refined with a constraint on the total integer occupancy of the positions and a restraint on the overall Re/Mo ratio of 5:1. The occupancies for structure **2** were refined without constraint, giving good agreements with the EDS results.

Selected crystal, collection, and refinement data for **1**−**4** are collected in Table S2. Selected interatomic bond distances for **1**−**4** can be found in Table S3. Crystallographic data for the structures of the title compounds have been deposited at the Cambridge Crystallographic Data Center as CCDC 2059019 for **1**, CCDC 2060965 for **2**, CCDC2059020 and 2059021 for **4** and **3**, respectively.

Computational Details. Density functional theory (DFT) calculations were carried out for the $[Re_5MoSe_8(CN)_6]^n$ (n = 3−, 4−, and 5−) cluster anions in the *ADF* program package.[56−58] The geometric parameters of the cluster anions in C_1 symmetry were preliminarily optimized with the PW92+revPBE density functional[59,60] and STO's all-electron TZ2P basis set.[61] The optimized structures were close to C_{4v} symmetry; thus, this symmetry was used to optimize the cluster anions with the B3LYP[62] hybrid density functional, Grimme D4(EEQ)[63] dispersion correction, and all-electron TZP basis set.[61] Single-point calculations with the B3LYP hybrid density functional, Grimme D4(EEQ) dispersion correction, and all-electron TZ2P basis set were performed afterward to achieve the properties of the systems.

The spin-unrestricted approximation was used for the $[Re_5MoSe_8(CN)_6]^{4-}$ cluster anion. The QTAIM charges and spin densities were calculated within the *ADF* package. The zero-order regular approximation (ZORA)[64] for the scalar relativistic effects and conductor-like screening model (COSMO) model[65] for the water environment were used in all calculations.

Preparation of $K_5[Re_5MoSe_8(CN)_6]\cdot 8H_2O$ (1). $MoSe_2$ (1.777 g, 7.00 mmol), $ReSe_2$ (2.409 g, 7.00 mmol), and KCN (4.023 g, 61.92 mmol) were ground and loaded into the quartz ampule, which was then evacuated, sealed, and heated at 650 °C for 2 weeks. After cooling, the ampule was opened in air and the reaction mixture was washed with deoxygenated water. The volume of the orange solution was reduced to 3 mL, and ethanol was added, causing precipitation of the orange powder of compound **1** in a yield of 700 mg (25% counting on $ReSe_2$). Single crystals of **1** suitable for X-ray structural analysis were grown by means of slow ethanol diffusion in a concentrated aqueous solution of **1** in a thin glass ampule narrowing in the middle. The heavy element ratio for **1** by EDS was 5.2:5.0:1.0:8.1 K/Re/Mo/Se. FT-IR (KBr, cm^{-1}): ν 2095 (C≡N). UV−vis absorption [H_2O; λ_{max}, nm (ε, M^{-1} cm^{-1})]: 230

(50840), 477 (454). The phase purity of the sample was confirmed by PXRD analysis (Figure S3a). The solid sample **1** is long-term stable during air exposure, showing no significant evolution of the PXRD powder patterns or sample color.

Preparation of (n-Bu_4N)$_4$[$Re_5MoSe_8(CN)_6$] (2). A total of 80 mg (0.04 mmol) of compound **1** was dissolved in water, and an aqueous solution of tetrabutylammonium bromide (150 mg, 0.47 mmol in 10 mL) was added. An aqueous solution of 0.1 M HCl was added dropwise to the resulting solution in order to facilitate oxidation of the cluster by O_2 until a precipitate formed. ***Caution!*** *One should preliminarily confirm the phase purity of* ***1*** *and avoid the KCN admixture because of the potential risk of formation hydrogen cyanide during the addition of an acid.* The precipitate was separated by centrifugation, dried in air, and recrystallized from acetone. Yield of **2**: 75 mg (74%). Crystals suitable for XRD were obtained by the slow diffusion of pentane vapor into solution **2** in acetone. The heavy element ratio for **2** by EDS was 4.9:1.1:7.4 Re/Mo/Se. Elem anal. Calcd for $C_{70}H_{144}N_{10}Se_8Mo_1Re_5$: C, 30.03; H, 5.19; N, 5.01. Found: C, 30.01; H, 5.11; N, 4.95. HR-ESI-MS (−, CH_2Cl_2). Calcd for $((n\text{-Bu})_4N)_2[Re_5MoSe_8(CN)_6]^{2-}$: *m*/*z* 1150.32. Found: *m*/*z* 1150.30 (100%). Calcd for $((n\text{-Bu})_4N)[Re_5MoSe_8(CN)_6]^{2-}$: *m*/*z* 1029.16. Found: *m*/*z* 1029.16 (65%). Calcd for $[Re_5MoSe_8(CN)_5]^{3-}$: *m*/*z* 605.34. Found: *m*/*z* 605.36 (18%). FT-IR (KBr, cm^{-1}): ν 2108 (CN), 2958, 2872, 1629, 1485, 1381, 1150, 883, 739 (most intensive bands for $[CH_3(CH_2)_3]_4N^+$). UV−vis absorption [CH_3CN; λ_{max}, nm (ε, M^{-1} cm^{-1})]: 232 (48560), 464 (724), 518 (573), 562 (894), 665 (193), 957 (411). The phase purity of the sample was confirmed by PXRD analysis (Figure S3b).

Preparation of (Ph_4P)$_4$[$Re_5MoSe_8(CN)_6$]·5DMF (3). A total of 200 mg (0.09 mmol) of compound **1** was dissolved in 10 mL of water, and an aqueous solution of bromine (0.08 M, about 1 mL) was added dropwise until the solution color changed from orange to red. Then a tetraphenylphosphonium bromide (200 mg, 0.48 mmol in 10 mL) solution was added dropwise until a precipitate formed. After complete decolorization of the solution, the precipitate was separated by centrifugation and dried in air. Yield of **3**: 270 mg (92%). Crystals suitable for XRD were obtained by the slow diffusion of diethyl ether vapor into solution **3** in *N*,*N*-dimethylformamide (DMF). The heavy element ratio for **3** by EDS was 4.1:4.9:1.1:8.2 P/Re/Mo/Se. Elem anal. Calcd for $C_{102}H_{80}N_6P_4Se_8Mo_1Re_5\cdot 0.5C_3H_7NO$: C, 38.8; H, 2.6; N, 2.8. Found: C, 38.5; H, 3.0; N, 2.5. FT-IR (KBr, cm^{-1}): ν 2104 (CN), 1585, 1483, 1437, 1107, 997, 756, 721, 689, 527 (most intensive bands for Ph_4P^+). UV−vis absorption [DMF; λ_{max}, nm (ε, M^{-1} cm^{-1})]: 464 (1035), 521 (862), 562 (1328), 660 (307), 952 (571).

Preparation of (Ph_4P)$_3$[$Re_5MoSe_8(CN)_6$] (4). A total of 200 mg (0.06 mmol) of compound **3** was dissolved in 10 mL of DMF, and the bromine solution in CH_2Cl_2 (0.073 M, 0.42 mL) was added dropwise until the solution from red to brown-violet. Then, 10 mL of isopropyl alcohol and water were added until precipitation occurred. The precipitate was filtered off, washed with isopropyl alcohol, and dried in air, yielding 93 mg (60%). Crystals suitable for XRD were obtained by the slow diffusion of diethyl ether vapor into solution **4** in CH_2Cl_2. The heavy element ratio for **4** by EDS was 3.4:4.9:1.1:8.3 P/Re/Mo/Se. Elem anal. Calcd for $C_{78}H_{60}N_6P_3Se_8Mo_1Re_5$: C, 33.1; H, 2.1; N, 3.0. Found: C, 32.7; H, 2.3; N, 3.1. FT-IR (KBr, cm^{-1}): ν 2120 (CN), 1585, 1483, 1437, 1105, 997, 756, 723, 689, 528 (most intensive bands for Ph_4P^+). UV−vis absorption [DMF; λ_{max}, nm (ε, M^{-1} cm^{-1})]: 276 (27060), 532 (941), 579 (1250).

■ RESULTS AND DISCUSSION

Synthesis. Our experiments of the reaction of rhenium and molybdenum diselenides with the potassium cyanide melt have shown that the composition of the cluster products depends both on the reaction temperature and on the degree of crystallinity of the selenides used. The use in the reaction of diselenides obtained at 600 °C and a sufficiently low reaction temperature (630 °C) leads to a similar reactivity of diselenides and the formation of a single cluster product, the chain polymeric compound $K_6[Re_3Mo_3Se_8(CN)_4(CN)_{2/2}]$ (Scheme 1 and eq 1), consisting mainly of the cluster core $\{Re_3Mo_3Se_8\}$.[46]

$$3MoSe_2 + 3ReSe_2 + 14KCN \rightarrow K_6[Re_3Mo_3Se_8(CN)_4(CN)_{2/2}] + \frac{9}{n}(CN)_n + 4K_2Se \quad (1)$$

Scheme 1. Preparation of $K_6[Re_3Mo_3Se_8(CN)_5]$[a]

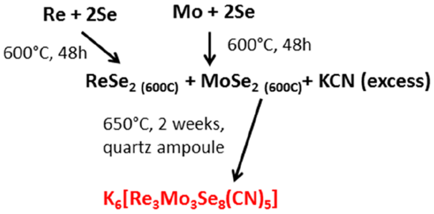

[a](600C) = subscript in the scheme indicating the diselenides preparation temperature in degrees Celsius.

If the reaction temperature is increased and/or if diselenides obtained at higher temperatures (with a higher degree of crystallinity) are used, it also leads to the $K_6[Re_{3.6}Mo_{2.4}Se_8(CN)_4(CN)_{2/2}]$ phase, isomorphic to the previously obtained one. However, part of molybdenum diselenide remains as the byproduct of the reaction.[66] Examination of the rinsing water by elemental analysis and MS showed that the reaction product contains, along with an excess of KCN and K_2Se, cluster complex-based compounds with a high Re content, namely, $K_5[Re_5MoSe_8(CN)_6]$ (25% yield counting on $ReSe_2$) with traces of $K_4[Re_6Se_8(CN)_6]$ (Scheme 2). The change of the reagent loading to 5:1 $ReSe_2$/$MoSe_2$ aimed at directly preparing the $K_5[Re_5MoSe_8(CN)_6]$ compound indeed led to an increase in the yield of $K_5[Re_5MoSe_8(CN)_6]$ up to 39%; however, it also caused a simultaneous increase of the content of the homometallic cluster $K_4[Re_6Se_8(CN)_6]$ up to 40%, complicating the separation process.

Scheme 2. Preparation of $K_5[Re_5MoSe_8(CN)_6]$[a]

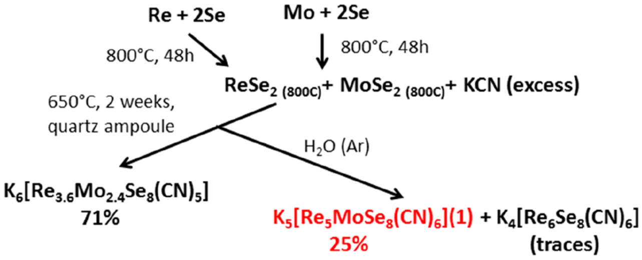

[a](800C) = subscript in the scheme indicating the diselenides preparation temperature in degrees Celsius.

Redox Properties. The CV curve for salt **2** in acetonitrile is characterized by two one-electron redox transitions (Figure 2, lower). The cathodic and anodic curves show that the ratio of i_{pc} and i_{pa} for the processes is close to 1. The first redox process with a $E_{1/2}$ value of −0.462 V is attributed to reversible oxidation of the cluster complex $[Re_5MoSe_8(CN)_6]^{5-}$ to $[Re_5MoSe_8(CN)_6]^{4-}$. The second process at 0.039 V accordingly reflects further reversible oxidation of the cluster complex $[Re_5MoSe_8(CN)_6]^{4-}$ with the formation of

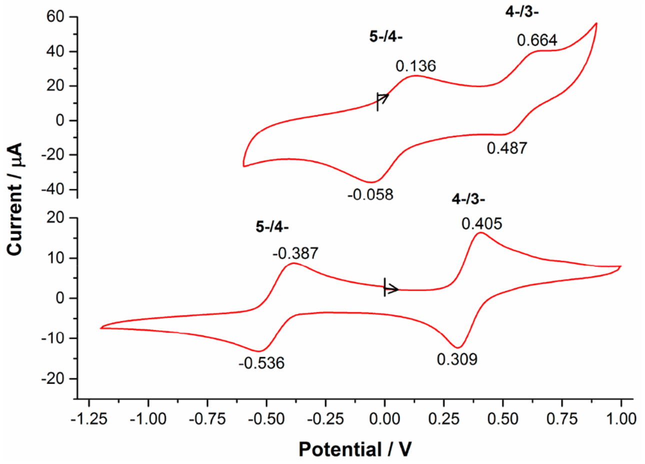

Figure 2. Cyclic voltammograms for **1** (upper) in H_2O and **2** (lower) in CH_3CN. The scan rate for **1** is 500 mV/s, and that for **2** is 200 mV/s. The potential is given versus Ag/AgCl.

$[Re_5MoSe_8(CN)_6]^{3-}$. The dependence of the CV shape on the scan rate is shown in Figure S4. The values of the currents and potentials for transitions depending on the scan rate are given in Table S1.

The Δ*E* values for all processes are significantly higher than the typical 59 mV for a single-electron "Nernstian" process.[67] The Δ*E* value measured varies from 90 to 200 mV (with 25−800 mV/s corresponding to the scan rate), which indicates a high energy barrier of the redox process and slow electron transfer. Homometallic octahedral chalcogenide cluster complexes also demonstrate high Δ*E* values that practically never correspond to the values typical for the "Nernstian" process.[18,41] The Δ*E* values of the ferrocene measured under similar conditions are also relatively large (117 mV obtained at the 25 mV/s scan rate; Figure S5). The effect of the scan rate, working electrode type, solvent, temperature, or uncompensated resistance on the Δ*E* values of the ferrocene is known.[68,69] Taking that into account, it cannot be excluded that large Δ*E* values for cluster complexes may arise from the setup and experimental conditions used for CV. The dependence of the cathodic current i_{pc} on $\nu^{1/2}$ according to the Randles−Sevcik equation[67] is linear for all observed processes (Figures S6 and S7).

For an aqueous solution of **1**, the voltammogram shows similar one-electron redox transitions (Figure 2, upper). However, noticeable deviations of the i_{pc} and i_{pa} ratio are observed for the transformation 3−/4− in an aqueous medium, depending strongly on the scan rate, which may indicate irreversible degradation of the oxidized product.[67]

As evidenced in Figure 2, the electrochemical potentials of the $[Re_5MoSe_8(CN)_6]^n$ cluster complex significantly depend on the nature of the solvent. In an acetonitrile solution, the $E_{1/2}$ values for the 4−/5− and 3−/4− transitions are −0.462 and 0.357 V. In an aqueous solution, the corresponding $E_{1/2}$ values are significantly shifted to higher values (0.029 and 0.577 V, respectively), which can be explained by solvation.[67,70,71] A similar effect was also observed for the rhenium cluster complex $[Re_6Se_8(CN)_6]^n$ (acetonitrile, −0.37 V;[40] water, −0.619 V[41]). The obtained $E_{1/2}$ values for the transitions for $[Re_5MoSe_8(CN)_6]^n$ in comparison with other rhenium/molybdenum chalcogenide clusters are given in Table 1.

The nonisoelectronic replacement of one Re atom with a Mo atom in the cluster core results in a higher charge of the cluster anions of the isoelectronic clusters, e.g., $[Re_5MoSe_8(CN)_6]^{5-}$ and $[Re_6Se_8(CN)_6]^{4-}$, both containing 24 CSE. The metal atom replacement also leads to the appearance of an additional oxidative transition of the heterometallic cluster complex. Hence, $[Re_5MoSe_8(CN)_6]^n$ can exist in three oxidation states (n = 3−, 4−, and 5−) compared to two for $[Re_6Se_8(CN)_6]^n$ (n = 3− and 4−).[42] The 24/23 CSE redox transition potential for the substituted Re/Mo cluster shifts to negative values compared to the rhenium one (−0.462 V for $[Re_5MoSe_8(CN)_6]^{4-/5-}$ and 0.37 V for $[Re_6Se_8(CN)_6]^{3-/4-}$ in CH_3CN). An increase in the number of Mo atoms in the cluster core leads to a further shift of the redox potentials to the negative values. The corresponding redox transition potentials (24/23 CSE) for the cluster complexes $[Re_4Mo_2Se_8(CN)_6]^{5-/6-}$ and $[Re_3Mo_3Se_8(CN)_6]^{6-/7-}$ are −1.294 and −1.410 V, respectively. Cluster complexes with a high content of molybdenum, i.e., $[Re_3Mo_3Se_8(CN)_6]^n$ and $[Mo_6Se_8(CN)_6]^n$, are involved in three oxidative transformations and can exist in four oxidation states. However, because of a strong shift in the potential values, cluster anions with high CSE content are very unstable with respect to oxidation and can be isolated only under excess of a reducing agent.[18]

Chemical Oxidation. The solid sample of **1** is long-term stable in air, while air exposure of an aqueous solution of **1** causes a solution color change from orange to red. The reaction in air is pH-dependent (eq 2 and Figure S8).

Table 1. $E_{1/2}$ **(V) Values from the CV Data for** $[Re_{6-x}Mo_xSe_8(CN)_6]^n$ **(x = 0−3, 6) Cluster Anions**[a]

	anion (solvent)/CSE number			
	20/21	21/22	22/23	23/24
$[Re_6Se_8(CN)_6]^n$ (CH_3CN)[40]				0.37 (3−/4−)
$[Re_6Se_8(CN)_6]^n$ (H_2O)[41]				0.619 (3−/4−)
$[Re_5MoSe_8(CN)_6]^n$ (CH_3CN)			0.357 (3−/4−)	−0.462 (4−/5−)
$[Re_5MoSe_8(CN)_6]^n$ (H_2O)			0.577 (3−/4−)	0.029 (4−/5−)
$[Re_4Mo_2Se_8(CN)_6]^n$ (CH_3CN)[66]			−0.476 (4−/5−)	−1.294 (5−/6−)
$[Re_3Mo_3Se_8(CN)_6]^n$ (CH_3CN)[66]		−0.202 (4−/5−)	−0.870 (5−/6−)	−1.270 (6−/7−)
$[Re_3Mo_3Se_8(CN)_6]^n$ (DMF)[46]		−0.325 (4−/5−)	−0.818 (5−/6−)	−1.410 (6−/7−)
$[Re_3Mo_3Se_8(CN)_6]^n$ (H_2O)			−0.490 (5−/6−)	
$[Mo_6Se_8(CN)_6]^n$ (H_2O)[18]	−0.647 (6−/7−)	−1.081 (7−/8−)	−1.574 (8−/9−)	

[a] Potentials are normalized versus Ag/AgCl/3.5 M KCl electrode. The cluster anion charges for the corresponding redox transition are given in parentheses.

$$[\mathrm{Re_5MoSe_8(CN)_6}]^{5-} + \frac{1}{4}\mathrm{O_2} + \mathrm{H^+} = [\mathrm{Re_5MoSe_8(CN)_6}]^{4-} + \frac{1}{2}\mathrm{H_2O} \qquad (2)$$

Oxidative spectrophotometric titration of the cluster complex $[\mathrm{Re_5MoSe_8(CN)_6}]^{5-}$ by bromine in an aqueous solution results in the evolution of absorption spectra (Figure 3). Further, the addition of bromine water leads to neither a position nor an intensity change of the characteristic absorption bands of the cluster complex, showing no further oxidation of the cluster complex in aqueous solution.

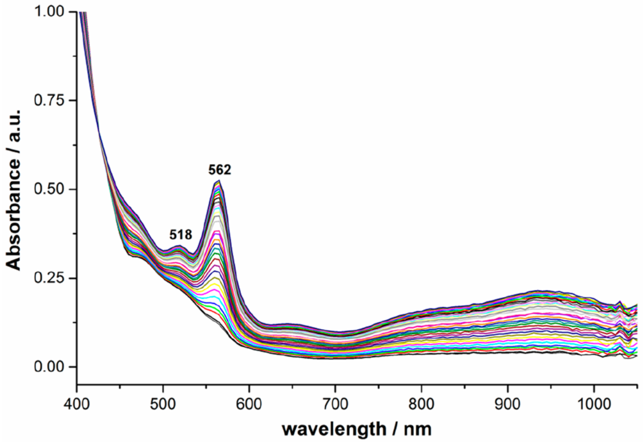

Figure 3. UV−vis absorbance spectra for compound **1** in H_2O during titration by a bromine aqueous solution.

The conditions for crystallization of the oxidized cluster in the form of a potassium salt from an aqueous solution were not found owing to the high solubility of the compound. A metathesis reaction with tetrabutylammonium bromide was used in order to isolate the cluster complex into the solid phase. The addition of a tetrabutylammonium bromide solution to an aqueous solution of **1**, followed by acidification, led to the precipitation of $(n\text{-}\mathrm{Bu_4N})_4[\mathrm{Re_5MoSe_8(CN)_6}]$ (**2**), which was structurally characterized. The resulting salt **2** is soluble in polar organic solvents. Figure 4 shows a fragment of the isotope distribution in the MS spectrum of an acetonitrile solution of compound **2**, corresponding to the adduct $\{(\mathrm{C_{16}H_{36}N})_2[\mathrm{Re_5MoSe_8(CN)_6}]\}^{2-}$. The detailed assignments of the ESI-MS data can be found in Figure S9.

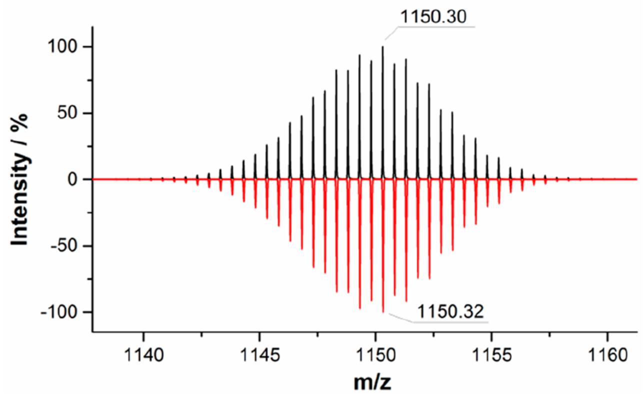

Figure 4. Selected isotopic distribution pattern in negative mode for an adduct of **2**, observed black curve versus calculated red for $\{(\mathrm{C_{16}H_{36}N})_2[\mathrm{Re_5MoSe_8(CN)_6}]\}^{2-}$.

Adding a solution of bromine in acetonitrile to an acetonitrile solution of **2** leads to further oxidation of the cluster complex and a solution color change from red to brown-violet. Oxidative spectrophotometric titration of the cluster $[\mathrm{Re_5MoSe_8(CN)_6}]^{4-}$ bromine in acetonitrile showed the evolution of absorption spectra during titration (Figure 5).

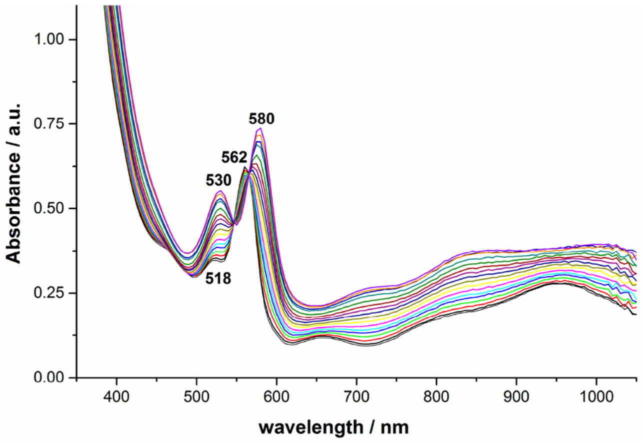

Figure 5. UV−vis absorbance spectra for compound **2** in CH_3CN during titration by bromine.

Attempts to crystallize the anion $[\mathrm{Re_5MoSe_8(CN)_6}]^{3-}$ with n-$\mathrm{Bu_4N^+}$ cations were not successful. A similar procedure for $\mathrm{Ph_4P^+}$ salt yields **4**, which was structurally characterized.

IR Spectroscopy. FT-IR spectra of **1**, **2**, and **4** revealed the characteristic CN vibration wavenumber to shift depending on the cluster CSE number. Compared with free cyanide (2080 $\mathrm{cm^{-1}}$),[72] the frequencies of the CN stretch vibrations of the cluster complex are shifted to higher energies, which indicates a significant contribution of the σ-donating interaction. The CN vibration for $[\mathrm{Re_5MoSe_8(CN)_6}]^{5-}$ occurs on 2099 $\mathrm{cm^{-1}}$ and shifts to 2104 $\mathrm{cm^{-1}}$ for $[\mathrm{Re_5MoSe_8(CN)_6}]^{4-}$ and to 2120 $\mathrm{cm^{-1}}$ for $[\mathrm{Re_5MoSe_8(CN)_6}]^{3-}$ (Figure S10). With oxidation of the cluster complex, the nominal charge of the metal atoms of the cluster becomes more positive, the σ-donating interaction becomes more efficient, and CN stretch becomes more pronounced.[72] A similar effect was observed for the cluster complexes of rhenium and molybdenum (2107 and 2130 $\mathrm{cm^{-1}}$ for $[\mathrm{Re_6Se_8(CN)_6}]^{4-}$[73] and $[\mathrm{Re_6Se_8(CN)_6}]^{3-}$,[42] respectively; 2080 and 2098 $\mathrm{cm^{-1}}$ for $[\mathrm{Mo_6Se_8(CN)_6}]^{7-}$ and $[\mathrm{Mo_6Se_8(CN)_6}]^{6-}$,[74] respectively).

EPR Spectroscopy. The EPR data showed that only the sample **2** was paramagnetic. The EPR spectrum for **2** has a shape typical for the case of axial anisotropy for $S = {}^1/_2$ and is characterized by two components of the g factor: $g_{\parallel} = 2.861$ and $g_{\perp} = 2.220$ (Figure 6). This shape of the spectrum is in good agreement with the axial symmetry of the singly occupied molecular orbital (SOMO; 386A, Figure 11). The simulated spectrum was obtained with a hyperfine coupling constant with the nuclear spin of rhenium $A(\mathrm{Re}) = 5$ mT ($I = {}^5/_2$, not resolved because of the low value of the constant). High values of the g factor are also characteristic for other chalcogenide cluster complexes [$g = 2.44$–2.56 for $[\mathrm{Re_6Q_8L_6}]^{3-}$ (Q = S, Se, Te; L = CN, Cl, Br);[75,76] $g = 2.430$ for $(\mathrm{Ph_4P})_4[\mathrm{Re_3Mo_3Se_8(CN)_6}]\cdot 2\mathrm{CH_3CN}$;[46] $g_{\perp} = 2.4425(1)$ and $g_{\parallel} = 1.9822(1)$ for $\mathrm{K_6[Mo_6Se_8(CN)_5]}$[77]]. For $\mathrm{K_6[Mo_6Se_8(CN)_5]}$ characterized by

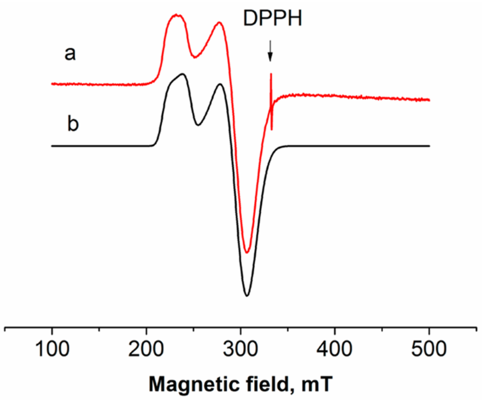

Figure 6. Experimental EPR spectra for compound **2** at 77 K with the addition of a DPPH standard (a) and simulated with a hyperfine structure constant of $A_{\parallel}(\mathrm{Re})$ = 5.0 mT (b).

a crystal structure built up on polymeric chains, a similar axial anisotropy of the paramagnetic signal is observed, which is consistent with the axial SOMO a_{1g}.[77]

Electronic Spectroscopy. The electronic absorption spectroscopy (EAS) spectra of heterometallic cluster anions $[Re_5MoSe_8(CN)_6]^n$ where n = 5− (**1**), 4− (**2**), and 3− (**4**) in solution (Figure 7) contain absorption bands in the UV region with high extinction values of 28000−50000 M^{-1} cm^{-1}. The position of the absorption maximum in the UV region weakly depends on the charge state of the cluster (230 nm for **1** and 232 nm for **2**). Comparison of the spectrum of **1** with those of **2** and **4** in the visible region revealed a noticeable difference in the absorption band numbers, maxima, and extinction. Solution colors vary from orange to pink and then to violet with respect to the cluster oxidation state (Figure 7). The spectra of the oxidized cluster complexes **2** and **4** exhibit broad absorption bands in the NIR region with maxima at 957 and 873 nm, respectively.

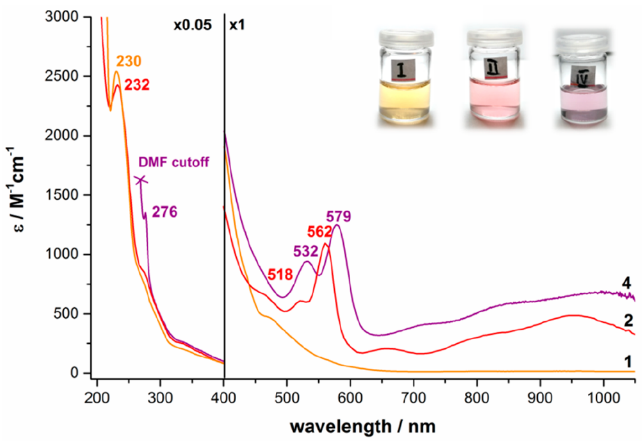

Figure 7. UV−vis absorbance spectra for **1** in H_2O, **2** in CH_3CN, and **4** in DMF. Inset: Photographic images of diluted solutions (C = 0.4−0.6 mM/L). The data in the 200−400 nm region are presented at 0.05× scale, and the data in the 401−1050 nm region are presented at normal 1× scale.

EAS for cluster salts have isosbestic points (**1** and **2** at 440 nm; **2** and **4** at 547 and 566 nm), which confirms a single reactant to a single product transformation without side reactions involving the cluster complex.

Similar absorption bands with high extinction in the UV region were also observed for the cluster complexes $[Re_4Mo_2Se_8(CN)_6]^{4-}$ (244 nm)[66] and $[Re_3Mo_3Se_8(CN)_6]^{5-/4-}$ (236 nm).[66] Chalcogenide cluster complexes $[Re_6Se_8(CN)_6]^{4-/3-}$, $[Re_3Mo_3Se_8(CN)_6]^{5-/4-}$, and $[Mo_6Se_8(CN)_6]^{8-/7-}$ also demonstrate drastic changes in the absorption bands in the visible region with oxidation of the cluster anion.[18,66] The appearance of broad absorption bands in the NIR region is characteristic of electron-deficient chalcogenide cluster complexes and was also observed for $[Re_6Se_8(CN)_6]^{3-}$ (875 nm),[43] $[Re_3Mo_3Se_8(CN)_6]^{5-}$ (788 nm), and $[Re_3Mo_3Se_8(CN)_6]^{4-}$ (820 and 922 nm).[46]

Similar characteristic bands are observed in the visible region of the DRS spectra for solid samples of compounds **1**, **2**, and **4** (Figure 8).

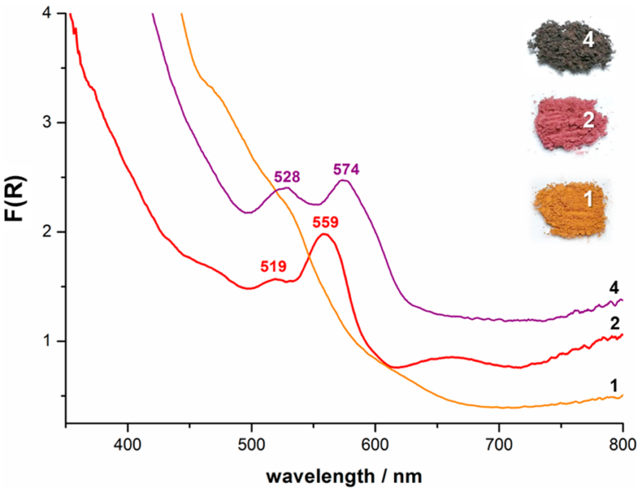

Figure 8. Kubelka−Munk transforms of the DRS spectra for compounds **1**, **2**, and **4**. Inset: Photographic images of the observed powder samples.

Cluster Core Electron Transitions. The weak dependence of the maxima and extinction of the absorption bands in the UV region on the oxidation state of the cluster complex indicates that the valence orbitals do not participate in the electronic transitions corresponding to this absorption. On the basis of calculations of the transition energy (230 nm corresponds to 5.4 eV), it can be assumed that this absorption corresponds to charge transfer from the low-lying bonding orbitals to an antibonding orbital block. High extinction values are associated with a large number of allowed transitions with close energies.

The effect of one-electron oxidation of the cluster complex on the position of the maximum and the transition extinction in the visible region indicates the strong connection of electronic transitions with the valence orbitals of cluster complexes. The presence of broad absorption bands in the NIR region only for electron-deficient cluster complexes indicates that the valence orbital, which becomes vacant during the oxidation process, is involved in transitions.

Crystal Structures. Structure 1. Compound **1** crystallizes in a cubic system with space group $Fm\bar{3}m$. The anionic part of the structure is represented by the anionic cluster-based complex $[Re_5MoSe_8(CN)_6]^{5-}$. The asymmetric unit contains one fully occupied cluster core metal position with a Re/Mo ratio of 5:1. The $\{Re_5Mo\}$ metal cluster core in the highly symmetric

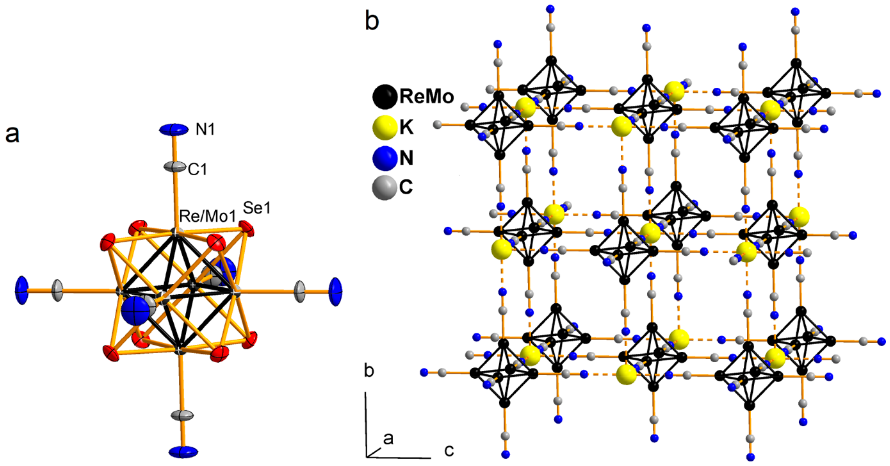

Figure 9. Structure of the cluster anion $[Re_5MoSe_8(CN)_6]^{5-}$ in **1** with thermal ellipsoids of 75% probability (a). Fragment of the crystal packing in **1**, in which Se atoms, K2 ions, and solvate water molecules are omitted for clarity (b).

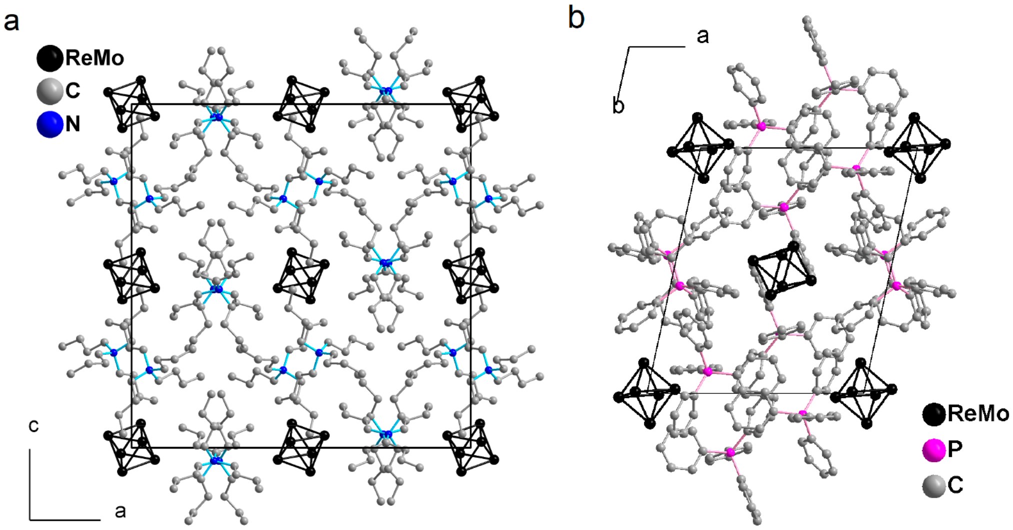

Figure 10. Unit cell structures in **2** (a) and **4** (b), in which cyanide ligands and Se and H atoms are omitted for clarity.

structure **1** is an ideal octahedron with an M−M bond distance of 2.644 Å.

Cluster anions are packed within the structure by ionic interactions between the cyanide ligand N atom and cations K1 with a K···N(C) distance of 2.740 Å. The cavities between close-packed cluster anions and K1 are taken up by the remaining cations K2 and O atoms from solvate water molecules. The structure of the cluster anion $[Re_5MoSe_8(CN)_6]^{5-}$ and the packing of $K_5[Re_5MoSe_8(CN)_6]\cdot 11H_2O$ are shown in Figure 9. Structure **1** is isomorphous to Prussian Blue (PB),[78] where the cluster complex is an expanded analogue of $[Fe(CN)_6]^n$ (n = 3− and 4−). Other cluster salts also are isomorphic to the PB structures $K_7[Mo_6Se_8(CN)_6]\cdot 8H_2O$[74] and $K_5[Re_3Mo_3Se_8(CN)_6]\cdot 11H_2O$.[46]

*Structure **2**.* Compound **2** crystallizes in an orthorhombic crystal system with space group *Pbca*. The asymmetric unit of the cluster anion of the structure contains three fully occupied cluster core metal positions, M1−M3. The refined ratios of Re and Mo were 0.854:0.146, 0.859:0.141, and 0.806:0.194 for the M1−M3 positions, respectively, with the total Re/Mo ratio in the resulting structure of 5:1 being in good agreement with the EDS results.

The cluster anions $[Re_5MoSe_8(CN)_6]^{4-}$ (23 CSE) and tetrabutylammonium cations form a close packing with cluster anions located at the vertices and centers of the unit cell faces. The structure of the unit cell in the *ac* projection is shown in Figure 10a.

The structure of **2** is isomorphic to n-Bu_4N^+ salts of other Re/Mo heterometallic cluster complexes $(n\text{-}Bu_4N)_4[Re_4Mo_2Se_8(CN)_6]$ and $(n\text{-}Bu_4N)_4[Re_3Mo_3Se_8(CN)_6]$,[66] containing cluster anions with the same charge.

*Structure **3**.* Compound **3** crystallizes in a triclinic system with space group $P\bar{1}$. The asymmetric unit of the cluster anion of the structure contains six metal positions, M1−M6. The occupancy of Re and Mo atoms was refined with a constraint on the total integer occupancy of the positions and a restraint on the overall Re/Mo ratio of 5:1 in accordance with the EDS data. The resulting structure contains cavities with solvate DMF molecules. The structure of the unit cell is shown in Figure S11.

*Structure **4**.* Compound **4** crystallizes in a triclinic system with space group $P\bar{1}$. The asymmetric unit of the cluster anion of the structure contains six core metal positions, M1−M6. The occupancy of Re and Mo atoms was refined with a constraint on

Table 2. Selected Interatomic Distances in the Selenocyanide Cluster Anions $[Re_{6-x}Mo_xSe_8(CN)_6]^n$ with Different CSE Numbers and Minimum−Maximum ⟨Mean⟩ Values (Å)

	CSE number	M−M min−max ⟨mean⟩, Å	M−Se min−max ⟨mean⟩, Å	M−C min−max ⟨mean⟩, Å	ref
$K_4[Re_6Se_8(CN)_6]\cdot 3.5H_2O$	24	2.624(1)−2.642(1) ⟨2.633(1)⟩	2.516(2)−2.538(2) ⟨2.526(2)⟩	2.09(2)−2.12(2) ⟨2.11⟩	73
$(Ph_4P)_4[Re_6Se_8(CN)_6]\cdot CH_3CN$	24	2.6329(5)−2.6452(5) ⟨2.639(5)⟩	2.5058(7)−2.5341(8) ⟨2.521(7)⟩	2.114(6)− 2.126(5) ⟨2.121(5)⟩	79
$(Ph_4P)_2H[Re_6Se_8(CN)_6]\cdot 8H_2O$	23	2.629−2.644 ⟨2.636(6)⟩	2.511−2.529 ⟨2.522(6)⟩	2.09−2.12 ⟨2.10(16)⟩	42
$(Ph_4P)_3[Re_6Se_8(CN)_6]\cdot CH_3CN\cdot H_2O$	23	2.6210(4)−2.6470(4) ⟨2.631(8)⟩	2.5070(7)−2.5330(7) ⟨2.521(7)⟩	2.089(6)−2.116(6) ⟨2.107(10)⟩	79
$K_5[Re_5MoSe_8(CN)_6]\cdot 8H_2O$ (**1**)	24	2.644(1)	2.530(1)	2.12(2)	present work
(n-$Bu_4N)_4[Re_5MoSe_8(CN)_6]$ (**2**)	23	2.6296(5)−2.6481(5) ⟨2.640(7)⟩	2.5163(9)−2.5401(9) ⟨2.529(8)⟩	2.120(10)−2.131(10) ⟨2.124(5)⟩	present work
$(Ph_4P)_4[Re_5MoSe_8(CN)_6]\cdot$ 5DMF (**3**)	23	2.6270(3)−2.6439(3) ⟨2.638(5)⟩	2.5169(5)−2.5394(5) ⟨2.529(7)⟩	2.122(5)−2.141(5) ⟨2.134(7)⟩	present work
$(Ph_4P)_3[Re_5MoSe_8(CN)_6]$ (**4**)	22	2.6159(5)−2.6438(5) ⟨2.634(10)⟩	2.5053(8)−2.5392(8) ⟨2.525(10)⟩	2.129(8)−2.131(9) ⟨2.140(8)⟩	present work
(n-$Bu_4N)_4[Re_4Mo_2Se_8(CN)_6]$	22	2.6274(6)−2.6659(6) ⟨2.65(1)⟩	2.523(1)−2.558(1) ⟨2.540(9)⟩	2.14(1)−2.20(1) ⟨2.16(2)⟩	66
$K_5[Re_3Mo_3Se_8(CN)_6]\cdot 11H_2O$	22	2.6494(9)	2.5464(9)	2.14(2)	46
$(Ph_4P)_4[Re_3Mo_3Se_8(CN)_6]\cdot 2CH_3CN$	21	2.6407(2)−2.6619(2) ⟨2.654(2)⟩	2.5197(3)−2.5463(3) ⟨2.539(7)⟩	2.164(3)−2.171(3) ⟨2.17(2)⟩	46
(n-$Bu_4N)_4[Re_3Mo_3Se_8(CN)_6]$	21	2.6417(10)−2.6697(10) ⟨2.656(9)⟩	2.5294(15)−2.5559(15) ⟨2.542(8)⟩	2.142(14)−2.188(15) ⟨2.16(2)⟩	66
$Na_8[Mo_6Se_8(CN)_6]\cdot 20H_2O$	22	2.6752(9)−2.7599(10) ⟨2.710⟩	2.559(1)−2.636(1) ⟨2.588⟩	2.182(8)	18
$K_7[Mo_6Se_8(CN)_6]\cdot 8H_2O$	21	2.700(3)	2.562(3)	2.17(2)	74
$(Me_4N)_4K_2[Mo_6Se_8(CN)_6]$ $10H_2O$	20	2.700(2)−2.721(2) ⟨2.711(2)⟩	2.568(2)−2.584(2) ⟨2.573(5)⟩	2.19(2)−2.21(1) ⟨2.20(2)⟩	74

the total integer occupancy of the positions and a restraint on the overall Re/Mo ratio of 5:1 in accordance with the EDS data.

The cluster anions $[Re_5MoSe_8(CN)_6]^{3-}$ (22 CSE) and tetraphenylphosphonium cations are close-packed, with the former located in the center of the *C* face and in the center of the *c* edges of the unit cell. The structure of the unit cell in the *ab* projection is shown in Figure 10b.

For the cluster complex $[Re_5MoSe_8(CN)_6]^n$, a decrease in the average interatomic distances in the cluster complex is observed with the removal of electrons from the cluster by varying the CSE number from 24 to 23 and 22. The M−M distances are shortened by ≈0.006 Å with each electron removed. In the heterometallic cluster series $[Re_{6-x}Mo_xSe_8(CN)_6]^n$, there is no uniform dependence of the average interatomic distances depending on the CSE number. An electronic state change leads to distortion of the cluster complex, which can ambiguously affect the average interatomic distances obtained from the structural data, as was confirmed in our previous study using extended X-ray absorption fine structure and DFT calculation data concerning the cluster complexes $[Re_3Mo_3Se_8(CN)_6]^n$ and $[Re_4Mo_2Se_8(CN)_6]^n$.[66] The overall geometry of the $[Re_5MoSe_8(CN)_6]^n$ cluster from the crystal data is slightly sensitive to the CSE number of the cluster. The average diagonal N−N and Se−Se distances are shortened only slightly with the CSE number decrease from 24 to 22 (N−N 10.312−10.284 Å and Se−Se 6.195−6.179 Å, respectively).

The interatomic distances M−M, M−Se, and M−C of the cluster complex $[Re_5MoSe_8(CN)_6]^n$ in the obtained crystal structures **1**−**4** are between the similar distances for $[Re_6Se_8(CN)_6]^n$ and $[Re_4Mo_2Se_8(CN)_6]^{4-}$ (Table 2). With an increase in Mo atoms in the composition of the cluster complex, an increase in the M−M, M−Se, and M−C average distances is observed. The average M−M distances are lengthened by ≈0.01 Å when one Re atom is replaced by a Mo one in the cluster core (when the isoelectronic cluster complexes are compared).

Electronic Structure of $[Re_5MoSe_8(CN)_6]^n$ (n = 5−, 4−, and 3−). To analyze the geometries and electronic structures of the heterometallic cluster complexes $[Re_5MoSe_8(CN)_6]^n$ (n = 5−, 4−, and 3−), quantum-chemical DFT calculations were performed. Near frontier orbitals mostly consisted of metal atomic orbitals and Se (Table S4). The changes in the molecular orbital energies for the $[Re_5MoSe_8(CN)_6]^n$ (n = 5−, 4−, and 3−) anions upon electron removal are shown in Figure 11.

The spin density in the open-shell $[Re_5MoSe_8(CN)_6]^{4-}$ cluster anion is primarily located on the M_6 core (Figure S12). Within the cluster core, most of the spin density is localized on the Mo (0.39) and Re (0.14) atoms in the apical positions. The amount of spin density is much higher on the Mo atom than on the Re atom. Thus, there is a strong polarization of the spin density along the *Z* axis, which leads to the axial anisotropy of the EPR spectra.

Local Symmetry of the Cluster Complex. The change in the electronic structure with the removal of electrons is accompanied by a change in the optimized geometry of the cluster anion. The 24-electron closed-shell metal cluster core $\{Re_5Mo\}$ is an almost ideal octahedron, where the M−M bond lengths are practically equal. The removal of electrons leads to a change in the bond lengths: a slight shortening of the Re−Re distances and a lengthening of the Re−Mo distances in the metal core (Figure 12a). The metal cores of anions containing 23 and 24 CSE numbers are weakly distorted, while the 22-electron anion demonstrates a more pronounced difference in the M−M distances in the cluster core. The removal of two electrons leads to a tetragonal distortion of the metal octahedron (Figure 12b). However, the metal core distortion shows practically no effect on the overall cluster anion geometry. The average diagonal N−N and Se−Se distances in the cluster are shortened only very slightly with a decrease in the CSE number from 24 to 22 (N−N 10.379−10.369 Å and Se−Se 6.278−6.271 Å).

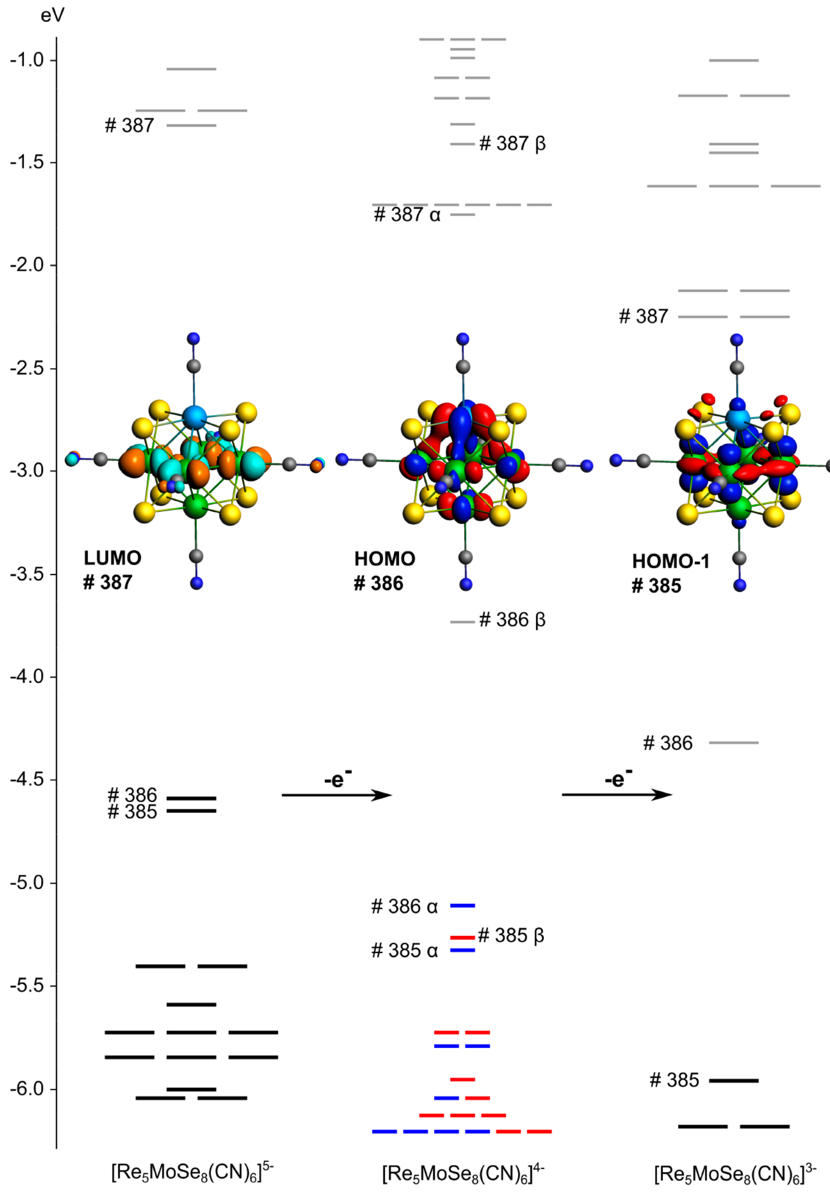

Figure 11. HOMO−1, HOMO, and LUMO molecular orbitals of the $[Re_5MoSe_8(CN)_6]^{5-}$ cluster anion and molecular-orbital-level diagrams for $[Re_5MoSe_8(CN)_6]^n$ upon electron removal. Doubly occupied orbitals, unoccupied orbitals, singly occupied α-orbitals, and singly occupied β-orbitals are marked by black, gray, blue, and red colors, respectively.

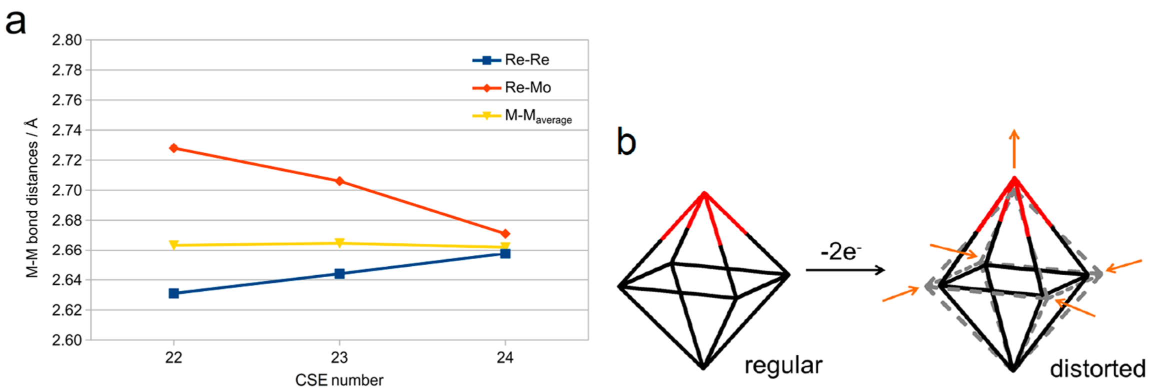

Figure 12. Analysis of the DFT-optimized M−M distances in the anions $[Re_5MoSe_8(CN)_6]^n$, where n = 5− (24 electrons), 4− (23 electrons), and 3− (22 electrons) (a). Distortion in the 22-electron $\{Re_5Mo\}$ metal core (b).

The local symmetry of the cluster complex in the crystal structures **1**−**4** is centrosymmetric, whereas the heterometallic anion $[Re_5MoSe_8(CN)_6]$ is C_{4v}-symmetric without an inversion center. The geometry of the cluster complex from the structural data is the result of averaging all possible orientations of the heterometallic core $\{Re_5MoSe_8\}$, resulting in partial occupation of the metal positions by Re and Mo in the cluster core.

■ CONCLUSION

A new electrochemically active cluster complex, $[Re_5MoSe_8(CN)_6]^{5-}$, undergoes two stepwise one-electron reversible oxidations. Moderate potentials allow us to separate electron-rich and electron-deficient forms in solution and in the solid state. DFT calculation data showed that the oxidation of the cluster complex leads to a slight distortion of the metal core without a substantial change in the overall geometry and ligand coordination. Cluster complexes exhibit UV absorption with large extinction values, which may be beneficial for UV-filtering coatings. Oxidation of the cluster complex causes a significant change in the extinction and position of the absorption band maxima in the visible and NIR regions. The electron-rich form (24 CSE) demonstrates weak absorption in the visible region, whereas oxidized species (23 and 22 CSE) comprise increased extinction values in the visible and NIR regions. The observed redox behavior and spectroscopic features of the novel heterometallic cluster complex make it promising in the field of electrochromic devices, light filters, and sensor materials.

■ ASSOCIATED CONTENT

Supporting Information

The Supporting Information is available free of charge at https://pubs.acs.org/doi/10.1021/acs.inorgchem.1c00763.

PXRD patterns, additional CV data, UV−vis in different pH values for **1**, IR spectra, MS data analysis, selected crystals, and collection and refinement data (PDF)

Accession Codes

CCDC 2059019−2059021 and 2060965 contain the supplementary crystallographic data for this paper. These data can be obtained free of charge via www.ccdc.cam.ac.uk/data_request/cif, or by emailing data_request@ccdc.cam.ac.uk, or by contacting The Cambridge Crystallographic Data Centre, 12 Union Road, Cambridge CB2 1EZ, UK; fax: +44 1223 336033.

■ AUTHOR INFORMATION

Corresponding Author

Viktoria K. Muravieva − *Nikolaev Institute of Inorganic Chemistry, Siberian Branch of the Russian Academy of Sciences (SB RAS), Novosibirsk 630090, Russia;* orcid.org/0000-0003-1103-2270; Email: muravyeva@niic.nsc.ru

Authors

Ivan P. Loginov − *Novosibirsk State University, Novosibirsk 630090, Russia*

Taisiya S. Sukhikh − *Nikolaev Institute of Inorganic Chemistry, Siberian Branch of the Russian Academy of Sciences (SB RAS), Novosibirsk 630090, Russia;* orcid.org/0000-0001-5269-9130

Maxim R. Ryzhikov − *Nikolaev Institute of Inorganic Chemistry, Siberian Branch of the Russian Academy of Sciences (SB RAS), Novosibirsk 630090, Russia*

Vadim V. Yanshole − *Novosibirsk State University, Novosibirsk 630090, Russia; International Tomography Center, Siberian Branch of the Russian Academy of Sciences (SB RAS), Novosibirsk 630090, Russia;* orcid.org/0000-0003-1512-3049

Vladimir A. Nadolinny − *Nikolaev Institute of Inorganic Chemistry, Siberian Branch of the Russian Academy of Sciences (SB RAS), Novosibirsk 630090, Russia*

Vincent Dorcet − *Institut des Sciences Chimiques de Rennes, CNRS, UMR 6226, Université Rennes, Rennes F-35000, France*

Stéphane Cordier − *Institut des Sciences Chimiques de Rennes, CNRS, UMR 6226, Université Rennes, Rennes F-35000, France;* orcid.org/0000-0003-0707-3774

Nikolay G. Naumov − *Nikolaev Institute of Inorganic Chemistry, Siberian Branch of the Russian Academy of Sciences (SB RAS), Novosibirsk 630090, Russia;* orcid.org/0000-0002-7531-6291

Complete contact information is available at:
https://pubs.acs.org/10.1021/acs.inorgchem.1c00763

Notes

The authors declare no competing financial interest.

■ ACKNOWLEDGMENTS

This work was supported by a grant from the Russian Science Foundation (Grant 20-73-00339). The authors thank the Collective Usage Center and XRD Facility of NIIC SB RAS for data collection. The authors acknowledge the International Research Project CLUSPOM between France and Russia and the “Centre de Diffractométrie X” of the Institute of Chemical Science of Rennes. The authors collective greatly thank A. A. Ulantikov and I. V. Ushina (NIIC) for measurements and analysis of CV and DRS. V.Y. thanks the Ministry of Science and Higher Education of the Russian Foundation for access to MS equipment.

■ REFERENCES

(1) Molard, Y.; Dorson, F.; Brylev, K. A.; Shestopalov, M. A.; Le Gal, Y.; Cordier, S.; Mironov, Y. V.; Kitamura, N.; Perrin, C. Red-NIR Luminescent Hybrid Poly(methyl methacrylate) Containing Covalently Linked Octahedral Rhenium Metallic Clusters. *Chem. - Eur. J.* **2010**, *16* (19), 5613−5619.

(2) Efremova, O. A.; Brylev, K. A.; Vorotnikov, Y. A.; Vejsadova, L.; Shestopalov, M. A.; Chimonides, G. F.; Mikes, P.; Topham, P. D.; Kim, S. J.; Kitamura, N.; Sutherland, A. J. Photoluminescent materials based on PMMA and a highly-emissive octahedral molybdenum metal cluster complex. *J. Mater. Chem. C* **2016**, *4* (3), 497−503.

(3) Krasilnikova, A. A.; Shestopalov, M. A.; Brylev, K. A.; Kirilova, I. A.; Khripko, O. P.; Zubareva, K. E.; Khripko, Y. I.; Podorognaya, V. T.; Shestopalova, L. V.; Fedorov, V. E.; Mironov, Y. V. Prospects of molybdenum and rhenium octahedral cluster complexes as X-ray contrast agents. *J. Inorg. Biochem.* **2015**, *144*, 13−17.

(4) Solovieva, A. O.; Kirakci, K.; Ivanov, A. A.; Kubat, P.; Pozmogova, T. N.; Miroshnichenko, S. M.; Vorontsova, E. V.; Chechushkov, A. V.; Trifonova, K. E.; Fufaeva, M. S.; Kretov, E. I.; Mironov, Y. V.; Poveshchenko, A. F.; Lang, K.; Shestopalov, M. A. Singlet Oxygen Production and Biological Activity of Hexanuclear Chalcocyanide Rhenium Cluster Complexes $[Re_6Q_8(CN)_6]^{4-}$ (Q = S, Se, Te). *Inorg. Chem.* **2017**, *56* (21), 13491−13499.

(5) Kirakci, K.; Zelenka, J.; Rumlova, M.; Martincik, J.; Nikl, M.; Ruml, T.; Lang, K. Octahedral molybdenum clusters as radiosensitizers for X-ray induced photodynamic therapy. *J. Mater. Chem. B* **2018**, *6* (26), 4301−4307.

(6) Kumar, P.; Kumar, S.; Cordier, S.; Paofai, S.; Boukherroub, R.; Jain, S. L. Photoreduction of CO_2 to methanol with hexanuclear

molybdenum $[Mo_6Br_{14}]^{2-}$ cluster units under visible light irradiation. *RSC Adv.* **2014**, *4* (20), 10420−10423.

(7) Feliz, M.; Atienzar, P.; Amela-Cortés, M.; Dumait, N.; Lemoine, P.; Molard, Y.; Cordier, S. Supramolecular Anchoring of Octahedral Molybdenum Clusters onto Graphene and Their Synergies in Photocatalytic Water Reduction. *Inorg. Chem.* **2019**, *58* (22), 15443−15454.

(8) Cordier, S.; Molard, Y.; Brylev, K.; Mironov, Y.; Grasset, F.; Fabre, B.; Naumov, N. Advances in the Engineering of Near Infrared Emitting Liquid Crystals and Copolymers, Extended Porous Frameworks, Theranostic Tools and Molecular Junctions Using Tailored Re6 Cluster Building Blocks. *J. Cluster Sci.* **2015**, *26*, 53−81.

(9) Cordier, S.; Grasset, F.; Molard, Y.; Amela-Cortes, M.; Boukherroub, R.; Ravaine, S.; Mortier, M.; Ohashi, N.; Saito, N.; Haneda, H. Inorganic Molybdenum Octahedral Nanosized Cluster Units, Versatile Functional Building Block for Nanoarchitectonics. *J. Inorg. Organomet. Polym. Mater.* **2015**, *25* (2), 189.

(10) Spreckelmeyer, B.; Schäfer, H. Die photometrische Titration des $[Ta_6Br_{12}]^{2+}$-Ions. *J. Less-Common Met.* **1967**, *13* (1), 127−129.

(11) Espenson, J. H.; McCarley, R. E. Oxidation of Tantalum Cluster Ions. *J. Am. Chem. Soc.* **1966**, *88* (5), 1063−1064.

(12) Saito, T.; Yoshikawa, A.; Yamagata, T.; Imoto, H.; Unoura, K. Synthesis, structure and electronic properties of octakis(.mu.3-sulfido)hexakis(triethylphosphine)hexatungsten as a tungsten analog of the molecular model for superconducting Chevrel phases. *Inorg. Chem.* **1989**, *28* (18), 3588−3592.

(13) Venkataraman, D.; Rayburn, L. L.; Hill, L. I.; Jin, S.; Malik, A.-S.; Turneau, K. J.; DiSalvo, F. J. An Improved High Yield Synthesis Procedure and Reactivity of W_6S_8(4-tert-butylpyridine)$_6$. *Inorg. Chem.* **1999**, *38* (4), 828−830.

(14) Tragl, S.; Ströbele, M.; Glaser, J.; Vicent, C.; Llusar, R.; Meyer, H. J. Compounds with the Electron-Rich $[W_6Cl_{18}]^{2-}$ Cluster Anion. *Inorg. Chem.* **2009**, *48* (8), 3825−3831.

(15) Mackay, R. A.; Schneider, R. F. Experimental evidence concerning the electronic structure of the Nb_6Cl_{12} cluster. *Inorg. Chem.* **1967**, *6* (3), 549−552.

(16) Klendworth, D. D.; Walton, R. A. Synthesis, characterization, and electrochemistry of tertiary phosphine complexes of niobium and tantalum halide clusters. *Inorg. Chem.* **1981**, *20* (4), 1151−1155.

(17) Saito, T.; Yamamoto, N.; Nagase, T.; Tsuboi, T.; Kobayashi, K.; Yamagata, T.; Imoto, H.; Unoura, K. Molecular models of the superconducting chevrel phases: syntheses and structures of $[Mo_6X_8(PEt_3)_6]$ and $[PPN][Mo_6X_8(PEt_3)_6]$ (X = S, Se; PPN = $(Ph_3P)_2N$). *Inorg. Chem.* **1990**, *29* (4), 764−770.

(18) Magliocchi, C.; Xie, X.; Hughbanks, T. Cyanide-Melt Synthesis of Reduced Molybdenum Selenide Clusters. *Inorg. Chem.* **2004**, *43* (6), 1902−1911.

(19) Kirakci, K.; Kubát, P.; Langmaier, J.; Polívka, T.; Fuciman, M.; Fejfarová, K.; Lang, K. A comparative study of the redox and excited state properties of $(n\text{-}Bu_4N)_2[Mo_6X_{14}]$ and $(n\text{-}Bu_4N)_2[Mo_6X_8(CF_3COO)_6]$ (X = Cl, Br, or I). *Dalton Trans.* **2013**, *42* (19), 7224−7232.

(20) Gabriel, J.-C. P.; Boubekeur, K.; Uriel, S.; Batail, P. Chemistry of Hexanuclear Rhenium Chalcohalide Clusters. *Chem. Rev.* **2001**, *101* (7), 2037−2066.

(21) Wilson, W. B.; Stark, K.; Johnson, D. B.; Ren, Y.; Ishida, H. X.; Cedeno, D. L.; Szczepura, L. F. Photophysical Properties of a Series of Rhenium Selenide Cluster Complexes Containing Nitrogen-Donor Ligands. *Eur. J. Inorg. Chem.* **2014**, *2014* (13), 2254−2261.

(22) Yoshimura, T.; Nagata, K.; Matsuda, A.; Omote, T.; Kino, Y.; Takayama, T.; Sekine, T.; Shinohara, A. Synthesis, structures, redox properties, and theoretical calculations of thiohalide capped octahedral hexanuclear technetium(III) clusters. *Dalton Trans.* **2019**, *48* (37), 14085−14095.

(23) Yoshimura, T.; Ikai, T.; Takayama, T.; Sekine, T.; Kino, Y.; Shinohara, A. Synthesis, Spectroscopic and Electrochemical Properties, and Electronic Structures of Octahedral Hexatechnetium(III) Clusters $[Tc_6Q_8(CN)_6]^{4-}$ (Q = S, Se). *Inorg. Chem.* **2010**, *49* (13), 5876−5882.

(24) Yoshimura, T.; Ikai, T.; Tooyama, Y.; Takayama, T.; Sekine, T.; Kino, Y.; Kirishima, A.; Sato, N.; Mitsugashira, T.; Takahashi, N.; Shinohara, A. Synthesis, Structures, and Properties of New Chalcogenide-Capped Octahedral Hexatechnetium(III) Complexes $[Tc_6S_8X_6]^{4-}$ (X = Br, I), $[Tc_6Se_8I_2]$, and $[Tc_6Te_{15}]$. *Eur. J. Inorg. Chem.* **2010**, *2010* (8), 1214−1219.

(25) Hussey, C. L.; Quigley, R.; Seddon, K. R. Electrochemical and Spectroscopic Characterization of $\{Ta_6Cl_{12}\}^{z+}$ Chloride Clusters in Acetonitrile and in The Aluminum Chloride-1-Methyl-3-ethylimidazolium Chloride Molten Salt. *Inorg. Chem.* **1995**, *34* (1), 370−377.

(26) Quigley, R.; Barnard, P. A.; Hussey, C. L.; Seddon, K. R. Electrochemical and spectroscopic characterization of niobium $\{Nb_6Cl_{12}\}^{z+}$ chloride clusters in the aluminum chloride-1-methyl-3-ethylimidazolium chloride molten salt. *Inorg. Chem.* **1992**, *31* (7), 1255−1261.

(27) Long, J. R.; McCarty, L. S.; Holm, R. H. A Solid-State Route to Molecular Clusters: Access to the Solution Chemistry of $[Re_6Q_8]^{2++}$ (Q = S, Se) Core-Containing Clusters via Dimensional Reduction. *J. Am. Chem. Soc.* **1996**, *118* (19), 4603−4616.

(28) Yoshimura, T.; Umakoshi, K.; Sasaki, Y.; Sykes, A. G. Synthesis, Structures, and Redox Properties of Octa(μ3-sulfido)hexarhenium(III) Complexes Having Terminal Pyridine Ligands. *Inorg. Chem.* **1999**, *38* (24), 5557−5564.

(29) Molard, Y.; Ledneva, A.; Amela-Cortes, M.; Circu, V.; Naumov, N. G.; Meriadec, C.; Artzner, F.; Cordier, S. Ionically Self-Assembled Clustomesogen with Switchable Magnetic/Luminescence Properties Containing $[Re_6Se_8(CN)_6]^{n-}$ (n = 3, 4) Anionic Clusters. *Chem. Mater.* **2011**, *23* (23), 5122−5130.

(30) Vorotnikova, N. A.; Vorotnikov, Y. A.; Novozhilov, I. N.; Syrokvashin, M. M.; Nadolinny, V. A.; Kuratieva, N. V.; Benoit, D. M.; Mironov, Y. V.; Walton, R. I.; Clarkson, G. J.; Kitamura, N.; Sutherland, A. J.; Shestopalov, M. A.; Efremova, O. A. 23-Electron Octahedral Molybdenum Cluster Complex $[\{Mo_6I_8\}Cl_6]^{-}$. *Inorg. Chem.* **2018**, *57* (2), 811−820.

(31) Renaud, A.; Wilmet, M.; Truong, T. G.; Seze, M.; Lemoine, P.; Dumait, N.; Chen, W.; Saito, N.; Ohsawa, T.; Uchikoshi, T.; Ohashi, N.; Cordier, S.; Grasset, F. Transparent tantalum cluster-based UV and IR blocking electrochromic devices. *J. Mater. Chem. C* **2017**, *5* (32), 8160−8168.

(32) Nguyen, T. K. N.; Renaud, A.; Wilmet, M.; Dumait, N.; Paofai, S.; Dierre, B.; Chen, W.; Ohashi, N.; Cordier, S.; Grasset, F.; Uchikoshi, T. New ultra-violet and near-infrared blocking filters for energy saving applications: fabrication of tantalum metal atom cluster-based nanocomposite thin films by electrophoretic deposition. *J. Mater. Chem. C* **2017**, *5* (40), 10477−10484.

(33) Hernández-Acevedoa, L.; Arratia-Pérez, R. Relativistic Electronic Structure of Molecular precursors: The Case of the $[Re_6Q_8(CN)_6]^{4-}$/$[Re_6Q_8(CN)_6]^{3-}$ (Q = S, Se) Redox Couples. *J. Chil. Chem. Soc.* **2003**, *48*, 125−128.

(34) Deluzet, A.; Duclusaud, H.; Sautet, P.; Borshch, S. A. Electronic Structure of Diamagnetic and Paramagnetic Hexanuclear Chalcohalide Clusters of Rhenium. *Inorg. Chem.* **2002**, *41* (9), 2537−2542.

(35) Honda, H.; Noro, T.; Tanaka, K.; Miyoshi, E. Theoretical study on electronic excitation spectra of Mo and Re cluster complexes: $[(Mo_6Cl_8)Cl_6]^{2-}$ and $[(Re_6S_8)Cl_6]^{4-}$. *J. Chem. Phys.* **2001**, *114* (24), 10791−10797.

(36) Gray, T. G. Divergent Electronic Structures of Isoelectronic Metalloclusters: Tungsten(II) Halides and Rhenium(III) Chalcogenide Halides. *Chem. - Eur. J.* **2009**, *15* (11), 2581−2593.

(37) Gray, T. G.; Rudzinski, C. M.; Meyer, E. E.; Holm, R. H.; Nocera, D. G. Spectroscopic and Photophysical Properties of Hexanuclear Rhenium(III) Chalcogenide Clusters. *J. Am. Chem. Soc.* **2003**, *125* (16), 4755−4770.

(38) Baranovski, V. I.; Korolkov, D. V. Electron density distribution, polarizability and bonding in the octahedral clusters $[Mo_6S_8(CN)_6]^{6-}$, $[Re_6S_8(CN)_6]^{4-}$ and $Rh_6(CO)_{16}$. *Polyhedron* **2004**, *23* (9), 1519−1526.

(39) Hill, L. I.; Jin, S.; Zhou, R.; Venkataraman, D.; DiSalvo, F. J. Synthesis and Characterization of Oxidized $W_6S_8L_6$ Clusters. *Inorg. Chem.* **2001**, *40* (12), 2660−2665.

(40) Yoshimura, T.; Ishizaka, S.; Sasaki, Y.; Kim, H.-B.; Kitamura, N.; Naumov, N. G.; Sokolov, M. N.; Fedorov, V. E. Unusual Capping Chalcogenide Dependence of the Luminescence Quantum Yield of the Hexarhenium(III) Cyano Complexes $[Re_6(\mu_3\text{-}E)_8(CN)_6]^{4-}$, $E^{2-} = Se^{2-} > S^{2-} > Te^{2-}$. *Chem. Lett.* **1999**, *28* (10), 1121−1122.

(41) Ivanov, A.; Falaise, C.; Abramov, P.; Shestopalov, M.; Kirakci, K.; Lang, K.; Moussawi, M.; Sokolov, M.; Naumov, N.; Floquet, S.; Landy, D.; Haouas, M.; Brylev, K.; Mironov, Y.; Molard, Y.; Cordier, S.; Cadot, E. Host-Guest Binding Hierarchy within Redox- and Luminescence-Responsive Supramolecular Self-Assembly Based on Chalcogenide Clusters and γ-Cyclodextrin. *Chem. - Eur. J.* **2018**, *24*, 13382.

(42) (a) Naumov, N. G.; Ostanina, E. V.; Virovets, A. V.; Schmidtman, M.; Müller, A.; Fedorov, V. E. 23-Electron Re_6 metal clusters: syntheses and crystal structures of $(Ph_4P)_3[Re_6S_8(CN)_6]$, $(Ph_4P)_2(H)[Re_6Se_8(CN)_6]\cdot 8H_2O$, and $(Et_4N)_2(H)[Re_6Te_8(CN)_6]\cdot 2H_2O$. *Russ. Chem. Bull.* **2002**, *51* (5), 866−871. (b) Naumov, N. G.; Ostanina, E. V.; Virovets, A. V.; Schmidtman, M.; Müller, A.; Fedorov, V. E. 23-Electron Re_6 metal clusters: syntheses and crystal structures of $(Ph_4P)_3[Re_6S_8(CN)_6]$, $(Ph_4P)_2(H)[Re_6Se_8(CN)_6]\cdot 8H_2O$, and $(Et_4N)_2(H)[Re_6Te_8(CN)_6]\cdot 2H_2O$. *Izv. Akad. Nauk, Ser. Khim.* **2002**, *5*, 799−803.

(43) Kozlova, S. G.; Gabuda, S. P.; Brylev, K. A.; Mironov, Y. V.; Fedorov, V. E. Electronic Spectra and DFT Calculations of Hexanuclear Chalcocyanide Rhenium Clusters. *J. Phys. Chem. A* **2004**, *108* (47), 10565−10567.

(44) Litvinova, Y. M.; Gayfulin, Y. M.; Kovalenko, K. A.; Samsonenko, D. G.; van Leusen, J.; Korolkov, I. V.; Fedin, V. P.; Mironov, Y. V. Multifunctional Metal-Organic Frameworks Based on Redox-Active Rhenium Octahedral Clusters. *Inorg. Chem.* **2018**, *57* (4), 2072−2084.

(45) Tulsky, E. G.; Crawford, N. R. M.; Baudron, S. A.; Batail, P.; Long, J. R. Cluster-to-metal magnetic coupling: Synthesis and characterization of 25-electron $[Re_{6-n}Os_nSe_8(CN)_6]$ (5-n)- (n = 1, 2) clusters and $\{Re_{6-n}Os_nSe_8CNCu(Me_6\,tren)_6\}^{9+}$ (n = 0, 1, 2) assemblies. *J. Am. Chem. Soc.* **2003**, *125* (50), 15543−15553.

(46) Muravieva, V. K.; Gayfulin, Y. M.; Ryzhikov, M. R.; Novozhilov, I. N.; Samsonenko, D. G.; Piryazev, D. A.; Yanshole, V. V.; Naumov, N. G. Mixed-metal clusters with a $\{Re_3Mo_3Se_8\}$ core: from a polymeric solid to soluble species with multiple redox transitions. *Dalton Trans.* **2018**, *47* (10), 3366−3377.

(47) Argun, A. A.; Aubert, P.-H.; Thompson, B. C.; Schwendeman, I.; Gaupp, C. L.; Hwang, J.; Pinto, N. J.; Tanner, D. B.; MacDiarmid, A. G.; Reynolds, J. R. Multicolored Electrochromism in Polymers: Structures and Devices. *Chem. Mater.* **2004**, *16* (23), 4401−4412.

(48) Kubelka−Munk equation. In *Encyclopedic Dictionary of Polymers*; Gooch, J. W., Ed.; Springer: New York, 2007.

(49) Kraus, W.; Nolze, G. Powder Cell - a program for the representation and manipulation of crystal structures and calculation of the resulting X-ray powder patterns. *J. Appl. Crystallogr.* **1996**, *29*, 301−303.

(50) *APEX3 program suite V2016.1-0*; Bruker AXS Inc.: Madison, WI, 2016.

(51) Sheldrick, G. M. *SAINT*, version 8.37A; Bruker AXS Inc.: Madison, WI, 2013.

(52) Sheldrick, G. M. *SADABS*, version 2014/5; Bruker AXS Inc.: Madison, WI, 2014.

(53) Sheldrick, G. M. SHELXT - Integrated space-group and crystal-structure determination. *Acta Crystallogr., Sect. A: Found. Adv.* **2015**, *71*, 3−8.

(54) Sheldrick, G. M. Crystal structure refinement with SHELXL. *Acta Crystallogr., Sect. C: Struct. Chem.* **2015**, *71*, 3−8.

(55) Dolomanov, O. V.; Bourhis, L. J.; Gildea, R. J.; Howard, J. A. K.; Puschmann, H. OLEX2: a complete structure solution, refinement and analysis program. *J. Appl. Crystallogr.* **2009**, *42* (2), 339−341.

(56) *ADF2017, SCM Theoretical Chemistry*; Vrije Universiteit: Amsterdam, The Netherlands, 2017; http://www.scm.com.

(57) te Velde, G.; Bickelhaupt, F. M.; Baerends, E. J.; Fonseca Guerra, C.; Van Gisbergen, S. J. A.; Snijders, J. G.; Ziegler, T. Chemistry with ADF. *J. Comput. Chem.* **2001**, *22* (9), 931−967.

(58) Fonseca Guerra, C.; Snijders, J. G.; Te Velde, G.; Baerends, E. J. Towards an order-N DFT method. *Theor. Chem. Acc.* **1998**, *99* (6), 391−403.

(59) Perdew, J. P.; Burke, K.; Ernzerhof, M. Generalized gradient approximation made simple. *Phys. Rev. Lett.* **1996**, *77* (18), 3865−3868.

(60) Perdew, J. P.; Wang, Y. Accurate And Simple Analytic Representation of the Electron-Gas Correlation-Energy. *Phys. Rev. B: Condens. Matter Mater. Phys.* **1992**, *45* (23), 13244−13249.

(61) Van Lenthe, E.; Baerends, E. J. Optimized slater-type basis sets for the elements 1−118. *J. Comput. Chem.* **2003**, *24* (9), 1142−1156.

(62) Stephens, P. J.; Devlin, F. J.; Chabalowski, C. F.; Frisch, M. J. Ab Initio Calculation of Vibrational Absorption and Circular Dichroism Spectra Using Density Functional Force Fields. *J. Phys. Chem.* **1994**, *98* (45), 11623−11627.

(63) Caldeweyher, E.; Ehlert, S.; Hansen, A.; Neugebauer, H.; Spicher, S.; Bannwarth, C.; Grimme, S. A generally applicable atomic-charge dependent London dispersion correction. *J. Chem. Phys.* **2019**, *150* (15), 154122.

(64) Van Lenthe, E.; Ehlers, A.; Baerends, E. J. Geometry optimizations in the zero order regular approximation for relativistic effects. *J. Chem. Phys.* **1999**, *110* (18), 8943−8953.

(65) Pye, C. C.; Ziegler, T. An implementation of the conductor-like screening model of solvation within the Amsterdam density functional package. *Theor. Chem. Acc.* **1999**, *101* (6), 396−408.

(66) Muravieva, V. K.; Gayfulin, Y. M.; Prestipino, C.; Lemoine, P.; Ryzhikov, M. R.; Yanshole, V. V.; Cordier, S.; Naumov, N. G. Tailoring Heterometallic Cluster Functional Building Blocks: Synthesis, Separation, Structural and DFT Studies of $[Re_{6-x}Mo_xSe_8(CN)_6]^{n-}$. *Chem. - Eur. J.* **2019**, *25* (66), 15040−15045.

(67) Bard, A. J.; Faulkner, L. R. Electrochemical Methods: Fundamentals and Applications. *Russian Journal of Electrochemistry*, 2nd ed.; Wiley: New York, 2002; Vol. 38, pp 1364−1365.

(68) Tsierkezos, N. G. Cyclic Voltammetric Studies of Ferrocene in Nonaqueous Solvents in the Temperature Range from 248.15 to 298.15 K. *J. Solution Chem.* **2007**, *36*, 289−302.

(69) Tsierkezos, N. G.; Ritter, U. Electrochemical impedance spectroscopy and cyclic voltammetry of ferrocene in acetonitrile/acetone system. *J. Appl. Electrochem.* **2010**, *40*, 409−417.

(70) Gritzner, G. Solvent effects on redox potentials: Studies in N-methylformamide. *J. Electroanal. Chem. Interfacial Electrochem.* **1983**, *144* (1), 259−277.

(71) Marcus, Y. Thermodynamic functions of transfer of single ions from water to nonaqueous and mixed solvents: Part 3 - Standard potentials of selected electrodes. *Pure Appl. Chem.* **1985**, *57* (8), 1129−1132.

(72) McAfee, L. Infrared and Raman Spectra of Inorganic and Coordination Compounds. 5th Edition (Nakamoto, Kazuo). *J. Chem. Educ.* **2000**, *77* (9), 1122.

(73) Naumov, N. G.; Virovets, A. V.; Podberezskaya, N. V.; Fedorov, V. E. Synthesis and crystal structure of $K_4[Re_6Se_8(CN)_6]\cdot 3.5H_2$. *J. Struct. Chem.* **1997**, *38* (5), 857−862.

(74) Mironov, Y. V.; Virovets, A. V.; Naumov, N. G.; Ikorskii, V. N.; Fedorov, V. E. Excision of the $\{Mo_6Se_8\}$ Cluster Core from a Chevrel Phase: Synthesis and Properties of the First Molybdenum Octahedral Cluster Selenocyanide Anions $[Mo_6Se_8(CN)_6]^{7-}$ and $[Mo_6Se_8(CN)_6]^{6-}$. *Chem. - Eur. J.* **2000**, *6* (8), 1361−1365.

(75) Guilbaud, C.; Deluzet, A.; Domercq, B.; Molinie, P.; Coulon, C.; Boubekeur, K.; Batail, P. $(n\text{-}Bu_4N)_3[Re_6S_8Cl_6]^{3-}$: synthesis and luminescence of the paramagnetic, open shell member of a hexanuclear chalcohalide cluster redox system. *Chem. Commun.* **1999**, No. 18, 1867−1868.

(76) Larina, T. V.; Ikorskii, V. N.; Vasenin, N. T.; Anufrienko, V. F.; Naumov, N. G.; Ostanina, E. V.; Fedorov, V. E. Electronic State of Rhenium Complexes with Octahedral Chalcocyanide Cluster Anions $[Re_6Q_8(CN)_6]^{3-}$ (Q = S, Se, Te). EPR and Magnetic Susceptibility Studies. *Russ. J. Coord. Chem.* **2002**, *28* (8), 554−556.

(77) Magliocchi, C.; Xie, X.; Hughbanks, T. A Cyanide-Bridged Chain of Mo_6Se_8 Clusters: A Product of Cyanide-Melt Cluster Synthesis. *Inorg. Chem.* **2000**, *39* (22), 5000−5001.

(78) Buser, H. J.; Schwarzenbach, D.; Petter, W.; Ludi, A. The crystal structure of Prussian Blue: $Fe_4[Fe(CN)_6]_3.xH_2O$. *Inorg. Chem.* **1977**, *16* (11), 2704−2710.

(79) Baudron, S. A.; Deluzet, A.; Boubekeur, K.; Batail, P. Jahn-Teller distortion of the open-shell 23-electron chalcogenide rhenium cluster cores in crystals of the series, $\{[Re_6Q_8]^{3++}(X^-)_6\}^{3-}$ (Q = S, Se; X = Cl, CN). *Chem. Commun.* **2002**, *18*, 2124−2125.